Communication

Single-Cut Phaseless Near-Field Measurements for Fast Antenna Testing

Fernando Rodríguez Varela, Belén Galocha Iragüen, and Manuel Sierra Castañer

***Abstract*— Single-cut techniques allow for fast antenna characterization by measuring and transforming to far-field individual pattern cuts instead of the full sphere. The cut fields are expanded in a reduced set of cylindrical coefficients, which can be used to accurately compute the far-field in the main pattern cuts for antennas with separable aperture distributions. This communication introduces a fast single-cut near-field to far-field transformation method using amplitude-only data. The technique is based on the measurement of the near-field magnitude in two concentric cuts and starts an iterative propagation process to retrieve their phases. This technique becomes a fast tool for antenna characterization when one is interested in a few cardinal plane cuts of the antenna and only magnitude measurements are available. The proposed single-cut phaseless technique is tested using simulated and measured data, and it shows its potential for fast and more reliable amplitude-only measurements.**

***Index Terms*— Amplitude-only, cylindrical wave expansion (CWE), fast measurements, phaseless, single-cut.**

I. Introduction

Spherical near-field antenna measurements [1]–[4] have been established as the most accurate techniques for general antenna testing. For a proper near-field to far-field transformation, the amplitude and phase of the complex near-field must be sampled in the complete sphere with angular increments inversely proportional to the AUT electrical size, which can lead to expensive and time-consuming measurement processes. In recent years, multiple efforts have been made to address such limitations. Achieving fast and amplitude-only spherical measurements becomes convenient for testing high antenna volumes [5] and reducing equipment and operating costs, in both industrial and research scenarios.

A straightforward method to reduce antenna measurement times is to exploit the natural symmetry exhibited by many antennas [6]. Perhaps the most drastic approach in this sense has been the single-cut transformation [7]–[10]. This technique is based on the fact that most antenna measurements are conducted to retrieve the radiation pattern on a few cardinal cuts, typically the E- and H-planes. Using cylindrical wave expansion (CWE) [11], it is possible to perform near-field to far-field transformations of the antenna individual pattern cuts, which tremendously saves time because instead of measuring the complete sphere, only a few cuts are acquired.

In parallel, phaseless near-field antenna measurements have received increasing interest in recent years [12]. The lack of phase information must be compensated by other means, which results in different phaseless techniques, such as interferometry [13], holography [14], and multiple scan surfaces [15]–[22]. The latter option has the advantage that it does not rely on extra hardware. After measuring the near-field on two surfaces, several nonlinear algorithms [23] can be applied to retrieve the phase and the far-field pattern.

As a contribution toward fast, cheap, and reliable antenna measurements, this communication introduces a single-cut near-field technique using amplitude-only information. The proposed method is based on measuring the AUT near-field amplitude in two concentric cuts of different radii. The measured fields can be expanded in a truncated set of "single-cut waves," which involves much fewer degrees of freedom and then the standard 3-D measurements. This facilitates the phase retrieval process, which is implemented by iteratively propagating the field between the cuts, as is usually done in traditional phaseless techniques [17], [18], [21], [22].

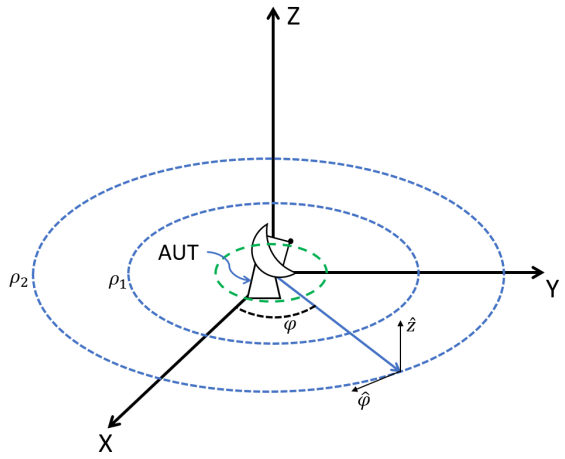

Fig. 1. Schematic representation of the geometry of a single-cut near-field antenna measurement scenario.

II. Theoretical Background

A. Single-Cut Near-Field to Far-Field Transformation

The cylindrical near-field measurement scenario of Fig. 1 with an AUT at the coordinate system origin is considered. The near-field of the antenna is described in cylindrical coordinates (ρ, ϕ, z). The tangential components of the electric field radiated by the antenna can be represented as a superposition of elementary cylindrical waves [11]. However, in single-cut techniques, the measurement is only performed in a $z = 0$ cut, which can be considered a cylinder of infinitesimal height [10]

$$\vec{E}(\rho, \phi, z) = \vec{E}(\rho, \phi)\,\delta(z) \tag{1}$$

where $\delta()$ is the Dirac delta function and $\vec{E}(\rho, \phi)$ is the field measured on the $z = 0$ cut. Inserting (1) into the CWE formulas

Manuscript received 25 November 2021; revised 31 March 2022; accepted 1 May 2022. Date of publication 30 May 2022; date of current version 9 November 2022. This work was supported by the Spanish Government, Ministry of Economy, National Program of Research, Development and Innovation through the Project New Array Antenna Technologies and Digital Processing for the FUTURE Integrated Terrestrial and Space-based Millimeter Wave Radio Systems–Integrated Terrestrial and Space-based Millimeter Wave Radio Systems for Future Communication Ecosystem beyond 5G (UPM-InTerSpaCE) under Grant PID2020-112545RB-C51. *(Corresponding author: Belén Galocha Iragüen.)*

The authors are with the Information Processing and Telecommunications Center, Radiation Group, Department of Signals, Systems and Radiocommunications, ETSI Telecomunicación, Universidad Politécnica de Madrid, 28040 Madrid, Spain (e-mail: belen@gr.ssr.upm.es).

Color versions of one or more figures in this communication are available at https://doi.org/10.1109/TAP.2022.3177525.

Digital Object Identifier 10.1109/TAP.2022.3177525

leads to the following transform pairs:

$$E_z(\rho,\phi) = \sum_{n=-N}^{N} k b_n H_n^{(2)}(k\rho)\, e^{jn\phi} \tag{2}$$

$$E_\phi(\rho,\phi) = -\sum_{n=-N}^{N} a_n \frac{\partial H_n^{(2)}}{\partial \rho} e^{jn\phi} \tag{3}$$

$$b_n k H_n^{(2)}(k\rho) = \frac{1}{2\pi}\int_{-\pi}^{\pi} E_z(\phi,\rho)\, e^{-jn\phi} d\phi \tag{4}$$

$$a_n \frac{\partial H_n^{(2)}}{\partial \rho}(k\rho) = -\frac{1}{2\pi}\int_{-\pi}^{\pi} E_\phi(\phi,\rho)\, e^{-jn\phi} d\phi \tag{5}$$

where the terms b_n and a_n are single-cut wave coefficients (SCWCs) and are closely related to the cylindrical wave coefficients but in one dimension. Finally, (2) and (3) can be asymptotically evaluated for $\rho \to \infty$ to retrieve the far-field pattern from SCWC [10].

Equations (2)–(5) can be used to perform near-field to far-field transformation of fields measured over a single-cut assuming the fields over a single-cut are independent of the other. In a general case, this assumption is not satisfied because all near-field cuts affect any far-field cut. However, many antennas exhibit a separable aperture field, which implies that the 2-D variations in the equivalent aperture fields can be split as the product of two 1-D variations [8]. This property enables accurate single-cut near-field to far-field transformations on the E- and H-planes. In these cuts, the contributions from the rest of the cuts tend to cancel each other, which results in low transformation errors [8].

B. Single-Cut Phaseless Algorithm

When only the field magnitude is measured, an alternative algorithm must be devised to retrieve the SCWC of the AUT. This can be solved by measuring the near-field amplitude signals on two cuts of different radii. Following an analogous approach to phaseless spherical measurements [17], an iterative propagation algorithm was selected to retrieve the phase. Although alternative nonlinear optimization algorithms have been proposed, our preliminary studies for spherical geometry [22] have shown that they tend to reconstruct the far-field with less accuracy.

The phase retrieval algorithm starts with the measured magnitudes on each cut. Then, an iterative algorithm [17] is started and propagates the electric field from one cut to the other. Each time the field is propagated to one cut, its amplitude is replaced by the one that has been measured. This process retrieves the phase of the field on both the cuts. When the retrieved phase stagnates to a point with negligible changes between consecutive iterations, convergence to the true solution or a local minimum has been achieved. This convergence occurs before 1000 iterations in all the simulations that we have performed.

Finally, the quality of the retrieved solution is evaluated with the normalized rms error of SCWC

$$\varepsilon_{comp} = \frac{\sqrt{\sum_{n=-N}^{N} |a_n - \tilde{a}_n|^2 + \left|b_n - \tilde{b}_n\right|^2}}{max\left(|a_n|, |b_n|\right)} \tag{6}$$

where $\tilde{a}_n$ and $\tilde{b}_n$ are the retrieved coefficients after the iterative process, and a_n and b_n are the true coefficients. Of course, this complex metric can only be computed when the SCWC of the AUT are *a priori* known, so it is not applicable to a real phaseless measurement scenario. However, it will be used in the simulation experiments in Section III.

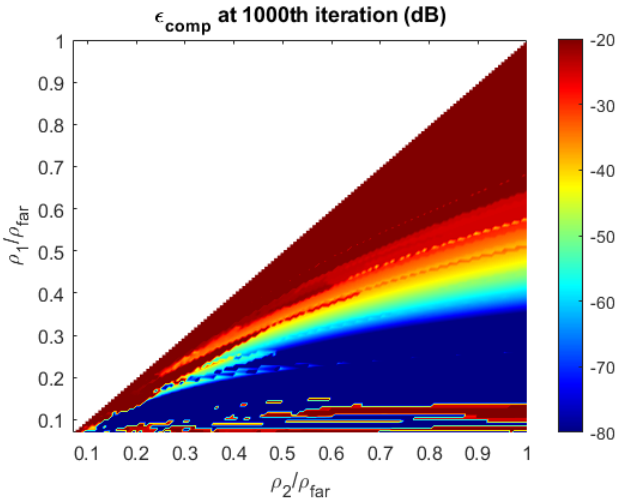

Fig. 2. Convergence error of phaseless single-cut measurements as a function of measurement radii.

III. Phaseless Single-Cut Transformation Results

Now, the phaseless single-cut technique is tested using a dipole-based simulation model. By arranging electric and magnetic dipoles in array configurations, AUTs of arbitrary size can be simulated with analytical equations to emulate aperture antennas. The near-field of a $D_y \times D_z = 10\lambda \times 10\lambda$ uniform array of Huygens sources is simulated on two concentric cuts with radii ρ_1 and ρ_2. The antenna is centered in the coordinate system origin over the YZ-plane with the main beam pointing in the $\hat{x}$-axis direction, so it is acquired by the measurement cuts. In all the experiments, an oversampling factor of 2 with respect to a standard single-cut (or cylindrical) measurement is used, since this has been reported [20] to improve the accuracy of phaseless techniques.

A. Influence of Measurement Radii

A set of simulations were performed by sweeping ρ_1 and ρ_2 between 10% and 100% of the AUT Rayleigh distance, $\rho_{far} = 182\lambda$. This normalization by ρ_{far} has been proposed in previous publications for spherical phaseless measurements [20] because it makes the obtained error plots independent of the AUT electrical size. For each combination of radii, the iterative phase retrieval algorithm introduced in Section II is evaluated for 1000 iterations.

Then, the metric ε_{comp} is calculated considering the SCWC obtained from a complex single-cut transformation as a reference. Fig. 2 depicts the resulting errors, where some combinations of measurement radii perform better than others. Both relative separation between measurement cuts and also the absolute values are important. In general, the algorithm tends to obtain very low error values as long as ρ_1 is approximately 15%–30% of ρ_{far} and ρ_2 has a separation of at least another 25%. There is a region of irregular behavior for low ρ_1 values, which has also been observed in previous publications for the spherical case [20], [21], but no explanation has been found.

B. Influence of AUT Size and Shape

A new set of simulations with different AUT sizes are performed in which the ρ_2 cut is swept between $0.1\rho_{far}$ and ρ_{far}. The other one is kept fixed to $\rho_1 = 0.35\rho_{far}$ because, as shown in Fig. 2, it is convenient that one of the cuts stays relatively near the AUT. A $5\lambda \times 5\lambda$ array with a Taylor distribution, and $15\lambda \times 5\lambda$ and $1\lambda \times 15\lambda$ uniform arrays are simulated for this test.

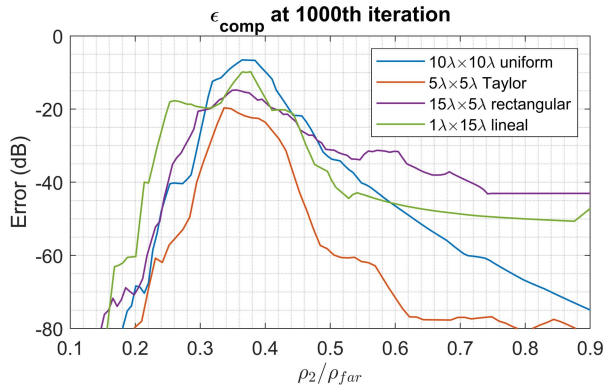

Fig. 3. Evolution of ϵ_{comp} as a function of measurement radius for several AUT types.

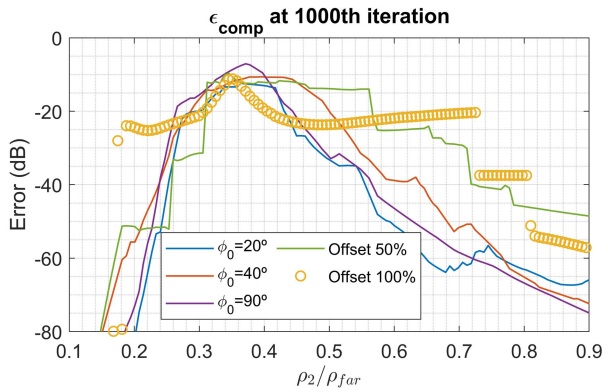

Fig. 4. Evolution of ϵ_{comp} as a function of measurement radius for several AUT pointing angles and offsets.

Fig. 3 depicts the obtained ε_{comp} errors of the retrieved solution, which shows a similar behavior with respect to the measurement radii as in the previous experiment. This validates the normalization approach to make the results independent of the antenna electrical size. The curves exhibit a somewhat irregular behavior with notably different error levels, but the general trend is a decreasing error with respect to the increasing separation between the cuts. This shows the robustness of the single-cut phaseless technique against antennas of different types and aspect ratios, in contrast to our previous investigations [20] on full spherical phaseless measurements where it was not possible to retrieve the phase of linear arrays.

C. Influence of the AUT Offset and Steering

The presence of beam steering and antenna offsets has been reported to degrade the accuracy of phaseless measurements [20], [21]. Therefore, a new set of simulations are performed to assess the influence of these parameters. The $10\lambda \times 10\lambda$ array is now fed with a linear phase taper to steer the beam in different ϕ_0 angles over the measured cut: 20°, 40°, and 90°. Additional simulations are performed by shifting the antenna from the coordinate system origin 5λ and 10λ (50% and 100% of the AUT size, respectively) along the $\hat{x}$-axis to emulate offset-mounted antenna measurements [24]. The obtained errors from the parametric sweep are depicted in Fig. 4, showing a nonlinear behavior due to the strong asymmetry created by the offset. This is translated into more irregular error plots, but the algorithm still can retrieve the phase for appropriate AUT probe separations.

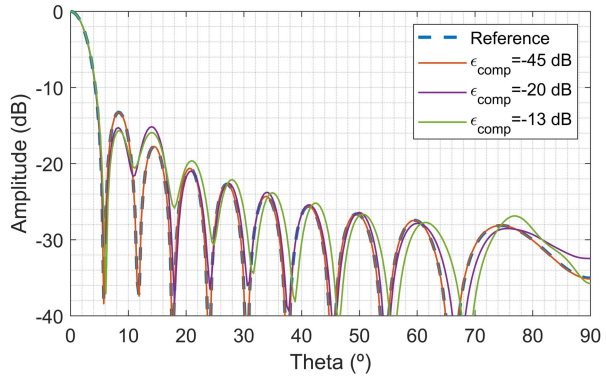

Fig. 5. Far-field amplitude patterns computed from several SCWC retrieved by the phaseless algorithm with different accuracies.

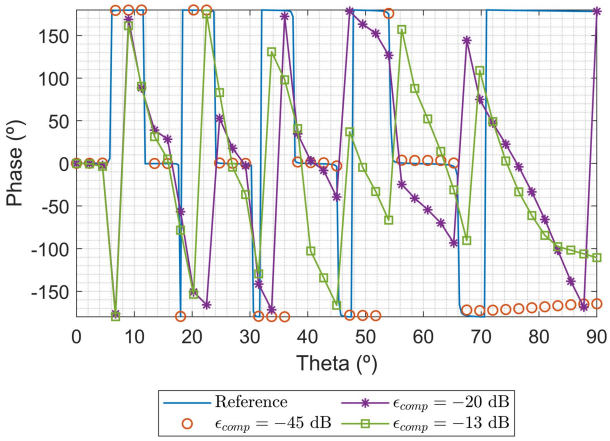

Fig. 6. Far-field phase patterns computed from several SCWCs retrieved by the phaseless algorithm with different accuracies.

D. Far-Field Pattern Analysis

Now the translation of ε_{comp} errors to the transformed radiation pattern is analyzed using the simulation data of the experiment in Fig. 3. The retrieved far-fields from the $10\lambda \times 10\lambda$ uniform array are depicted in Figs. 5 and 6 for ρ_2 values of $0.24\rho_{far}$, $0.31\rho_{far}$, and $0.32\rho_{far}$, which correspond to ϵ_{comp} levels of -45, -20, and -13 dB, respectively. The far-field pattern obtained from a single-cut complex measurement has also been depicted for use as a reference. The pattern amplitude is consistent with the reference even for high values of complex error. Meanwhile, the phase exhibits more discrepancies. This is an inherent characteristic of the iterative propagation technique and also observed in previous experiments for the spherical case [22], where relatively accurate far-field pattern magnitudes were obtained, even when complex error metrics were high.

IV. Phaseless Antenna Measurements

Now, the single-cut phaseless near-field to far-field transformation technique is tested using measured data. The measurements were performed in the anechoic chamber of the Technical University of Madrid (UPM). The spherical range used consists of a roll-over-azimuth positioner with a translation stage to perform spherical measurements with radii of 3–5.5 m.

A. 20 GHz Parabolic Reflector

The first antenna to be tested is a 20 GHz reflector antenna of 53 cm diameter with linear polarization and approximately 40 dBi of gain.

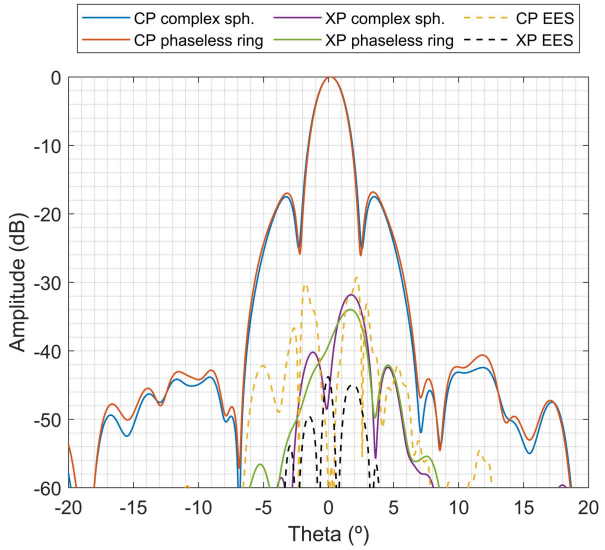

Fig. 7. Far-field patterns ($\phi = 0°$) obtained by the phaseless single-cut technique and spherical reference from SNIFT for the 20 GHz reflector.

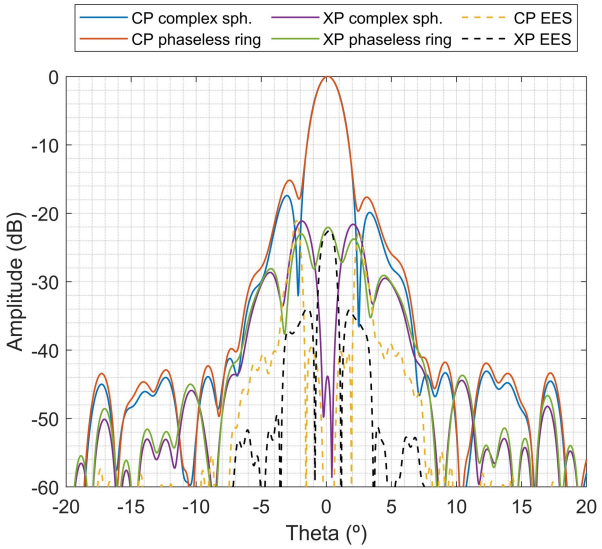

Fig. 8. Far-field patterns ($\phi = 45°$) obtained by the phaseless single-cut technique and spherical reference from SNIFT for the 20 GHz reflector.

Two complex spherical near-field measurements were performed at 3 and 5.5 m, each with two orthogonal orientations of a conical horn probe. An angular step of 1° is selected to obtain some level of oversampling to improve the quality of phase retrieval. Using the full spherical data, the far-field for both the spheres is computed with the commercial software SNIFT [25]. The average of both the patterns is used as a reference for phaseless measurements.

As discussed in Section III, the measurement radii play a significant role in the accuracy of single-cut phaseless measurements. The selected radii for this experiment correspond to 8% and 15% of the Rayleigh distance, respectively, which is somewhat near the optimal region of Fig. 2. Furthermore, both the measurement radii in electrical dimensions are larger than 200λ, where the single-cut approximations show small errors [10].

Two sets of phaseless single-cut measurements are generated by extracting $\phi = 0°$ and $\phi = 45°$ cuts of the spherical near-field data for both polarizations and spheres. One thousand iterations of the phaseless single-cut technique are performed for each of cut pair. The retrieved far-field patterns are depicted in Figs. 7 and 8, along with the equivalent error signal (EES) [20]. Both the patterns exhibit good consistency with the reference, but significant differences are appreciated in $\phi = 45°$ cut. This is a well-known limitation of single-cut measurements [10]. Nevertheless, the quality of reconstruction is remarkable considering the challenges of working with amplitude-only data.

B. DTU-ESA mmVAST Antenna

The second AUT is the DTU-ESA millimeter-wave validation standard antenna (mmVAST) [26], which is an offset single-reflector antenna with an astigmatic paraboloid having different focal lengths in the orthogonal offset and transverse planes. The resulting radiation pattern makes mmVAST a challenging test for near-field postprocessing techniques. The antenna has an aperture dimension of 230 mm × 230 mm, and the measurements are performed at 37.8 GHz in its circular polarization configuration.

The AUT is measured again in two spheres of radii 3 and 5.5 m with 0.5° angular increments and two orthogonal probe orientations. From each sphere, two orthogonal cuts corresponding to the antenna main planes $\phi = 0°$ and $\phi = 90°$ are extracted. The field amplitude

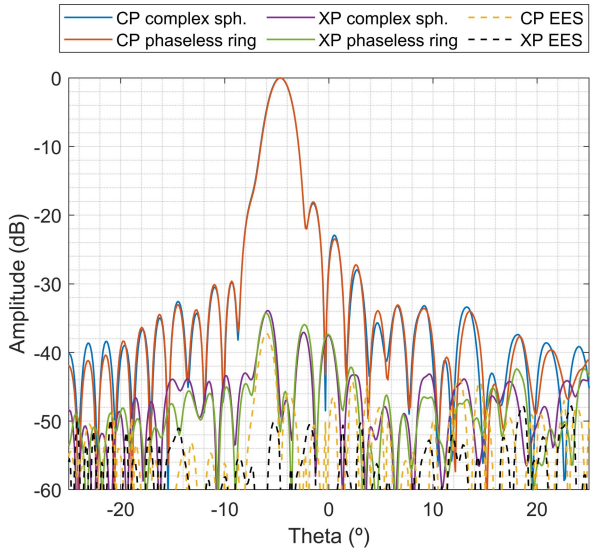

Fig. 9. Far-field patterns ($\phi = 0°$) obtained by the phaseless single-cut technique and spherical reference from SNIFT for mmVAST.

on these cuts is used for the phase retrieval algorithm, which is evaluated for 1000 iterations. The full spherical field is processed with SNIFT again to obtain a true reference far-field.

Figs. 9 and 10 depict the far-field patterns in the principal planes retrieved by both the approaches. For $\phi = 0°$ plane, the accuracy of phaseless single-cut transformation is remarkable with EES levels below -40 dB for both circular polarizations. Meanwhile, the asymmetry of this cut degrades the separability of the aperture. Such degradation is translated in a worse reconstruction of $\phi = 90°$ plane with EES values growing up to -20 dB.

C. Final Discussion

Table I shows a summary of the measurement time and accuracy of different measurement methods conducted for both AUTs, in its complex/phaseless and spherical/single-cut variants. The accuracy is assessed by integrating the EES over the entire angular range

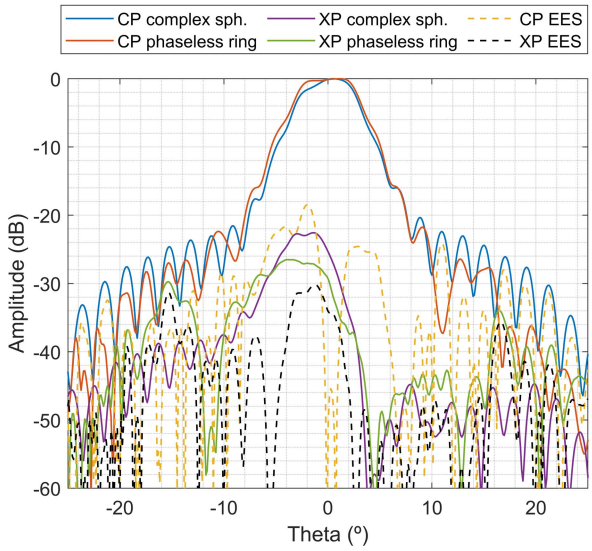

Fig. 10. Far-field patterns ($\phi = 90°$) obtained by the phaseless single-cut technique and spherical reference from SNIFT for mmVAST.

TABLE I
MEASUREMENT TIMES AND EES

AUT	Configuration	Meas. time	EES
20 GHz Reflector	Spherical complex	4 h 40 min	-
	Spherical phaseless	9 h 20 min	-50.3 dB
	Single-cut complex	2 min	-51.0 dB
	Single-cut phaseless	5 min	-50.1 dB
mmVAST	Spherical complex	12 h	-
	Spherical phaseless	24 h	-37.0 dB
	Single-cut complex	2 min	-53.5 dB
	Single-cut phaseless	5 min	-43.8 dB

considering the complex spherical measurement as a reference. The measurement time savings of the single-cut approach become drastic with only a small price to pay in the accuracy. The phaseless variant takes more time because it requires two cuts, but it is still negligible with respect to a full sphere scanning. The spherical phaseless results have been gathered from our previous publication [20], which were also obtained using the well-known iterative propagation phaseless algorithm.

For the 20 GHz reflector antenna experiment, the single-cut and spherical measurements show similar accuracy when working with phaseless data (around -50 dB of EES). Having full sphere near-field data allow for an exact postprocessing but phase retrieval introduces an error. On the other hand, phase retrieval of the single-cut measurement has been simplified, thanks to a reduced number of unknowns, but it suffers from the lack of separability in the single-cut approximation. In the end, both the sources of errors limit the maximum accuracy to approximately -50 dB.

The phase retrieval of mmVAST is more challenging due to the asymmetric pattern, which limits the accuracy of the spherical measurement to -37 dB. Here, the benefits of using a single-cut transformation become evident, since the reduced dimensionality enables the phaseless algorithm to reach an EES level of -43 dB. In this case, the lack of separability introduces an error of -53.5 dB when working with complex cut data. However, this error is lower than that obtained in both single-cut and sphere phaseless techniques; thus, it becomes a secondary issue.

These results demonstrate the potential capabilities of single-cut measurements in phaseless scenarios as a more reliable and faster tool than phaseless spherical measurements. The errors due to the lack of separability and phase reference prevent this technique from being used as a general and reliable tool in high-accuracy applications. However, this technique is very suitable for industrial applications where it is convenient to sacrifice some accuracy to maximize the antenna measurement speed.

The use of single-cut approaches to reduce measurement time in phaseless scenarios has been proposed before [27]. However, in those cases, phase retrieval was still solved in a 2-D domain after generating virtual measurement surfaces using the separability of the radiated fields. With the technique introduced in this communication, the number of unknowns involved in the phaseless problem is drastically reduced, which minimizes the chances of falling into local minima or false solutions [28].

V. CONCLUSION

This communication has introduced a new single-cut phaseless near-field to far-field transformation technique. The use of SCWCs as a 1-D field basis minimizes the number of unknowns during the phase retrieval process. As a result, the presence of local minima and false solutions typically encountered in traditional phaseless techniques is mitigated. This has been validated with numerical examples of different antenna types, orientations, and offsets, which show high robustness when measuring near-field magnitudes in two cuts with sufficient separation. The proposed algorithm has been tested with antenna measurements and obtains obtaining good consistency with full spherical complex measurements and drastic time savings.

REFERENCES

[1] *IEEE Recommended Practice for Near-Field Antenna Measurements*, IEEE Standard 1720-2012, Dec. 2012, pp. 1–102.
[2] *IEEE Standard Test Procedures for Antennas*, ANSI-IEEE Standard 149-1979, Nov. 1979, pp. 1–144.
[3] J. E. Hansen, *Spherical Near-Field Antenna Measurements*. London, U.K.: Peter Peregrinus, 1988.
[4] O. Breinbjerg, "Spherical near-field antenna measurements—The most accurate antenna measurement technique," in *Proc. IEEE Int. Symp. Antennas Propag. (APSURSI)*, Jun. 2016, pp. 1019–1020.
[5] F. R. Varela *et al.*, "Multi-probe measurement system based on single-cut transformation for fast testing of linear arrays," *Sensors*, vol. 21, no. 5, p. 1744, Mar. 2021.
[6] F. R. Varela, B. G. Iragüen, and M. Sierra-Castañer, "Under-sampled spherical near-field antenna measurements with error estimation," *IEEE Trans. Antennas Propag.*, vol. 68, no. 8, pp. 6364–6371, Aug. 2020.
[7] S. Omi, T. Uno, and T. Arima, "Single-cut near-field far-field transformation technique employing two-dimensional plane-wave expansion," *IEEE Antennas Wireless Propag. Lett.*, vol. 17, no. 8, pp. 1538–1541, Aug. 2018.
[8] Y. Sugimoto, H. Arai, T. Maruyama, M. Nasuno, M. Hirose, and S. Kurokawa, "Fast far-field estimation method by compact single cut near-field measurements for electrically long antenna array," *IEEE Trans. Antennas Propag.*, vol. 66, no. 11, pp. 5859–5868, Nov. 2018.
[9] R. Cornelius, T. Salmeron-Ruiz, F. Saccardi, L. Foged, D. Heberling, and M. Sierra-Castaner, "A comparison of different methods for fast single-cut near-to-far-field transformation," *IEEE Antennas Propag. Mag.*, vol. 56, no. 2, pp. 252–261, Apr. 2014.
[10] T. Salmeron-Ruiz, M. Sierra-Castaner, F. Saccardi, S. Burgos, F. J. Cano-Facila, and L. J. Foged, "A fast single cut spherical near-field-to-far-field transformation using cylindrical modes," in *Proc. 8th Eur. Conf. Antennas Propag. (EuCAP)*, Apr. 2014, pp. 2476–2480.
[11] O. M. Bucci and C. Gennarelli, "Use of sampling expansions in near-field-far-field transformation: The cylindrical case," *IEEE Trans. Antennas Propag.*, vol. AP-36, no. 6, pp. 830–835, Jun. 1988.
[12] O. Breinbjerg and J. F. Álvarez, "Phaseless near-field antenna measurement techniques—An overview," in *Proc. 38th Annu. Symp. Antenna Meas. Techn. Assoc. (AMTA)*, 2016, pp. 314–319.
[13] M. D. Migliore and G. Panariello, "A comparison of interferometric methods applied to array diagnosis from near-field data," *IEE Proc.-Microw., Antennas Propag.*, vol. 148, no. 4, pp. 261–267, Aug. 2001.

[14] J. L. Martínez, A. Arboleya-Arboleya, Y. Álvarez-López, C. García-González, and F. Las-Heras, "Phaseless antenna diagnostics based on off-axis holography with synthetic reference wave," *IEEE Antennas Wireless Propag. Lett.*, vol. 13, pp. 43–46, 2014.

[15] O. M. Bucci, G. D'Elia, G. Leone, and R. Pierri, "Far-field pattern determination from the near-field amplitude on two surfaces," *IEEE Trans. Antennas Propag.*, vol. 38, no. 11, pp. 1772–1779, Nov. 1990.

[16] R. G. Yaccarino and Y. Rahmat-Samii, "Phaseless bi-polar planar near-field measurements and diagnostics of array antennas," *IEEE Trans. Antennas Propag.*, vol. 47, no. 3, pp. 574–583, Mar. 1999.

[17] C. H. Schmidt, S. F. Razavi, T. F. Eibert, and Y. Rahmat-Samii, "Phaseless spherical near-field antenna measurements for low and medium gain antennas," *Adv. Radio Sci.*, vol. 8, pp. 43–48, Sep. 2010.

[18] J. F. Alvarez, J. M. Bjørstorp, and O. Breinbjerg, "Spherical phaseless probe-corrected near-field measurements of the DTU-ESA VAST12 reflector antenna," in *Proc. 40th Annu. Meeting Symp. Antenna Meas. Techn. Assoc.*, 2018, pp. 216–221.

[19] A. Bangun, C. Culotta-López, A. Behboodi, R. Mathar, and D. Heberling, "On phaseless spherical near-field antenna measurements," in *Proc. 13th Eur. Conf. Antennas Propag. (EuCAP)*, Mar. 2019, pp. 1–5.

[20] F. R. Varela, J. F. Álvarez, B. G. Iragüen, M. S. Castañer, and O. Breinbjerg, "Numerical and experimental investigation of phaseless spherical near-field antenna measurements," *IEEE Trans. Antennas Propag.*, vol. 69, no. 12, pp. 8830–8841, Dec. 2021.

[21] F. R. Varela, B. G. Iraguen, M. S. Castaner, J. F. Alvarez, M. Mattes, and O. Breinbjerg, "Combination of spherical and planar scanning for phaseless near-field antenna measurements," in *Proc. Antenna Meas. Techn. Assoc. Symp. (AMTA)*, Oct. 2019, pp. 1–6.

[22] F. R. Varela, B. G. Iragüen, and M. S. Castañer, "Practical considerations in phaseless spherical near-field measurements," in *Proc. Antenna Meas. Techn. Assoc. Symp. (AMTA)*, Oct. 2021, pp. 1–5.

[23] R. Chandra, T. Goldstein, and C. Studer, "PhasePack: A phase retrieval library," in *Proc. 13th Int. Conf. Sampling Theory Appl. (SampTA)*, Jul. 2019, pp. 1–5.

[24] F. R. Varela, B. G. Iragüen, and M. S. Castañer, "Fast spherical near-field to far-field transformation for offset-mounted antenna measurements," *IEEE Antennas Wireless Propag. Lett.*, vol. 19, no. 12, pp. 2255–2259, Dec. 2020.

[25] TICRA, Copenhagen, Denmark. *SNIFT Software*. Accessed: May 27, 2022. [Online]. Available: https://www.ticra.com/

[26] O. S. Kim *et al.*, "DTU-ESA millimeter-wave validation standard antenna (mm-VAST)-detailed design," in *Proc. 9th Eur. Conf. Antennas Propag. (EuCAP)*, Apr. 2015, pp. 1–4.

[27] R. Suzuki and H. Arai, "Reducing sampling points for estimating far-field from phaseless planar near-field with probe-positioning error," *IEICE Commun. Exp.*, vol. 6, no. 6, pp. 281–285, 2017.

[28] R. Pierri and R. Moretta, "On data increasing in phase retrieval via quadratic inversion: Flattening manifold and local minima," *IEEE Trans. Antennas Propag.*, vol. 68, no. 12, pp. 8104–8113, Dec. 2020.